# Numerical simulation of RHIC polarized proton run 17 spin flipper experiments

F. Méot, P. Adams, H. Huang, J. Kewisch, P. Oddo, and T. Roser
*Brookhaven National Laboratory, Upton, New York 11973, USA*

(Received 16 May 2024; accepted 10 June 2024; published 9 July 2024)

RHIC nine-magnet spin flipper has been operated successfully during RHIC polarized proton Run 17, with 97% spin flip efficiency achieved. The results show the importance of mirror resonance removal, small spin tune spread, and proper spin flipper driving tune sweep speed. Detailed spin tracking simulations, based on a Lorentz force and Thomas-BMT differential equation numerical solver code for accuracy, have been carried out to understand the experimental results. Agreement within measurement accuracy is obtained at injection energy, 23.8 GeV. It is not as tight at 255 GeV, reasons for that are exposed. These measurements and numerical studies allow to determine the sensitivity of spin-flip efficiency to the dispersion slopes at the two Siberian snakes and to the ac dipole frequency sweep speed. They also provide guidance for future developments at BNL's electron-ion collider.

DOI: 10.1103/PhysRevAccelBeams.27.071002

## I. INTRODUCTION

Spin physics programs at the future electron-ion collider at the Brookhaven National Laboratory [1] require measurement of bunch polarization with great accuracy, which includes reducing systematic errors. This can be achieved using a spin flipper [2–4], a device that allows multiple bunch polarization reversal during store while leaving the beam parameters and machine settings unchanged.

A spin flipper has been operated successfully, for the first time, during dedicated Accelerator Physics EXperiments (APEX in the following) during RHIC run 17 [4]. The details of the polarized proton acceleration chain in RHIC are shown in Fig. 1. RHIC lattice includes a pair of full Siberian snakes [5], which preserves beam polarization during the ramp and determines the operational spin tune (number of spin precessions per turn) $\nu_s = 1/2$. The nine-magnet spin flipper installed in IP ten straight in RHIC blue ring is sketched in Fig. 2, it is designed to induce an isolated spin resonance at $\nu_s = 1/2$.

The design, implementation, and operation parameters of the RHIC spin flipper have been supported all the way by spin dynamics simulations [2–4,6–8]. These are needed in order to account for the various potential limitations to spin flip efficiency, which are discussed in the following and include in particular possible excitation of the image resonance due to spin flipper defects and multiple crossing of the spin resonance which impacts on the validity domain of Froissart-Stora formula [9]. This numerical approach allows to analyze the outcomes of the 2017 APEX and to work out optimal parameter values for future experiments. It requires reproducing closely the conditions of run 17 experiments by setting up a realistic computer model [8], this will be addressed in detail in the next sections. An additional objective of the present simulations is to ensure spin tracking tools efficiency, as part of the ongoing code development efforts for the design of the electron-ion collider [10]. For this reason, many details of the spin flipper simulation method and outcomes are discussed.

As highest accuracy on particle and spin dynamics is required to simulate possible faint depolarizing effects (such as spin flipper defects exciting the image resonance, near-multiple crossing due to spin tune oscillations,

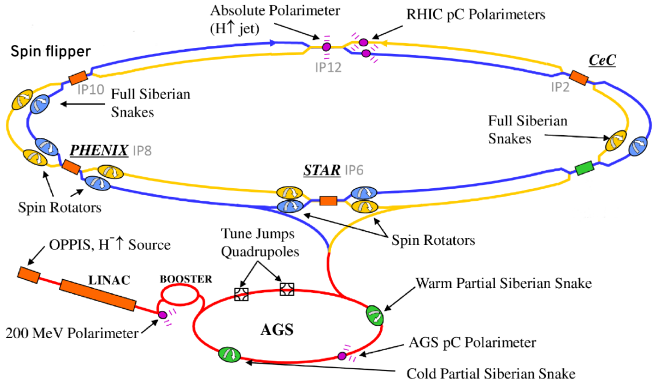


FIG. 1. Schematic layout of RHIC polarized proton acceleration complex. RHIC consists of two rings, named, respectively, blue ring (clockwise) and yellow ring (counterclockwise).

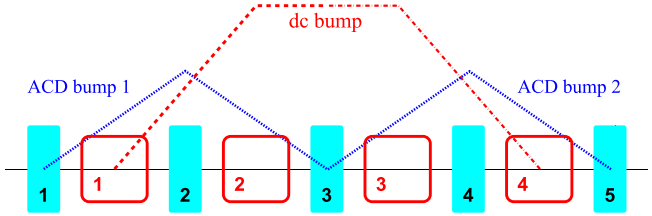


FIG. 2. A sketch of RHIC spin flipper. Dashed line (red): static horizontal orbit bump using dc spin rotators (numbered 1 to 4). Dotted line (blue): time-varying vertical orbit bumps from ac dipoles (numbered 1 to 5). The central ac dipole (3) is actually split, ACD bump 1 and ACD bump 2 are operated with a phase difference [Eq. (4)].

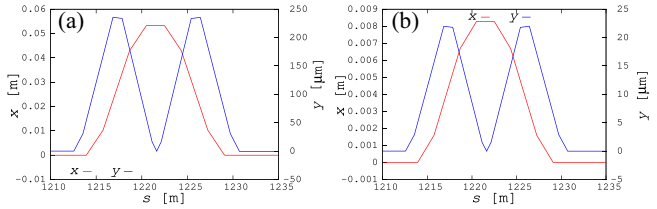


FIG. 3. Geometry of the horizontal (red curve and left vertical axes) and of the vertical (blue and right axes) orbit bumps over the spin flipper extent $1213 \lesssim s \lesssim 1231$ m, in the maximum amplitude configuration here. (a) 23.8 GeV, (b) 255 GeV.

nonlinear snake resonances), a Lorentz force and Thomas-BMT differential equation numerical solver code is used, as it intrinsically accounts for high-order particle coordinates, and for this very reason used for RHIC polarization studies over the past 15 years and in the electron-ion collider ion and electron spin polarization studies over the past 10 years [11].

The paper is organized as follows: Sec. II recalls the basic principles of RHIC spin flipper. Section III describes the working hypotheses, namely, RHIC optics as well as the spin flipper settings during the run 17 APEX and their implementation in the numerical model of the experiment. Preliminary basic simulations are produced in Sec. IV, aimed mostly at verifying that the model is implemented correctly. Section V details the APEX simulations and their outcomes and provides comparisons with APEX results. An Appendix gives additional simulation details regarding RHIC optics and rf settings (Appendix A), orbit defects (Appendix B), and spin dynamics (Appendixes B and C).

## II. SPIN FLIPPER IN RHIC

We briefly recall here aspects of RHIC spin flipper and its installation in RHIC, and of the underlying theory, relevant to the questions specifically addressed in this report. Additional details can be found in Refs. [2–8].

RHIC spin flipper extends over 18 m from $s = 1213$ to 1231 m clockwise (taking $s = 0$ at IP6) (Fig. 1). It is an interleave of four horizontal dipoles and five vertical ac dipoles (Fig. 2).

The four $y$ rotator (vertical field) dc dipoles with field integral $B_{\rm dc}L$ yield spin rotation angles $+\psi_0/-\psi_0/-\psi_0/+\psi_0$ respectively, with

$$\psi_0 = (1+G\gamma)\frac{B_{\rm dc}L}{B\rho}, \tag{1}$$

where $B\rho$ is the particle rigidity. Orbitwise, this defines a closed local horizontal bump (Fig. 3) and, spinwise, it leaves the spin tune $\nu_{\rm s} \approx 1/2$ unchanged (spin rotations sum up to zero).

The horizontal magnetic field in the ac dipoles has the form

$$B_{\rm osc}(t) = \hat{B}_{\rm osc}(t)\cos(2\pi f_{\rm osc}(t)t + \varphi_0), \tag{2}$$

with $f_{\rm osc}(t) = \nu_{\rm osc}(t) f_{\rm rev}$ the time-varying oscillation frequency and $\varphi_0$ a reference phase. $\hat{B}_{\rm osc}(t)$ is ramped to its peak value prior to sweeping $f_{\rm osc}(t)/f_{\rm rev}$ over a $\Delta\nu_{\rm osc}$ span, and then down, both ramps took place in 1.5 s in the APEX but in a much shorter time in the simulations. ACD1-3 and ACD3-5 dipole triplets, with dipole field integral $B_{\rm osc}l$, both ensure the same $+\phi_{\rm osc}(t)/-2\phi_{\rm osc}(t)/+\phi_{\rm osc}(t)$ spin $x$-rotation sequence, with

$$\phi_{\rm osc}(t) = (1+G\gamma)\frac{B_{\rm osc}(t)l}{B\rho}. \tag{3}$$

Orbitwise, each triplet ensures a locally closed vertical orbit bump (Fig. 3). The phases of the first (ACD1-3) and second (ACD3-5) vertical bumps are correlated, they need to satisfy

$$\varphi_{0,\text{ACD1-3}} - \varphi_{0,\text{ACD3-5}} = \psi_0. \tag{4}$$

This configuration of the ac dipole assembly induces a spin resonance at time $t$ when $\nu_{\rm osc}(t) = \nu_{\rm s}$. The phase relationship [Eq. (4)] causes the cancellation of the image resonance at $1-\nu_{\rm s}$, therefore, ensuring single resonance crossing and full spin flip, a paramount property as isolated resonance crossing in the presence of the image resonance instead, would require moving $\nu_{\rm s}$ away enough from $1/2$ which is not viable at RHIC [2].

The strength of the spin resonance is

$$\epsilon = \frac{\phi_{\rm osc}}{\pi}\sin\psi_0 \sin\frac{\psi_0}{2}. \tag{5}$$

The crossing speed (rate of sweep of $\nu_{\rm osc}$ through $\nu_{\rm s} \approx 1/2$) is a constant,

$$\alpha = \frac{\Delta\nu_{\rm osc}}{2\pi\tau_X f_{\rm rev}} \tag{6}$$

with $\tau_X$ the duration of the sweep. Single resonance crossing during the spin flip satisfies the Froissart-Stora formula [9],

$$\frac{P_f}{P_i} = 2\exp^{-\frac{\pi}{2}\frac{|\epsilon|^2}{\alpha}} - 1 = 2\exp^{-\frac{1}{2}\frac{\tau_X}{T}} - 1 \tag{7}$$

$P_i$ and $P_f$ are the initial and asymptotic polarizations, respectively. The $\tau_X$ dependent form is obtained by introducing

$$T = \frac{\Delta\nu_{\rm osc}}{2\pi^2\epsilon^2 f_{\rm rev}} \tag{8}$$

$T/\tau_X$ is presumably a small quantity at optimal flip efficiency (see Table II: $T/\tau_X \approx 0.06$ at 23.8 GeV, ≈0.04 at 255 GeV) so that $P_f/P_i \approx -1$.

The crossing speed $\alpha$ has to be small enough (sweep duration $\tau_X$ large enough) for spins to flip coherently so that $P_f/P_i \approx -1$. For instance, a series of ten flips over a few-hour store, with an overall polarization decrease not exceeding 1%, would require a flip efficiency $|P_f/P_i| \approx 99.9\%$, this sets an upper threshold for $\alpha$. On the other hand, a limit on the lower value of $\alpha$ is expected due to the aforementioned multiple resonance crossing, an effect that has its origin in momentum-dependent spin tune oscillation, as follows.

*Spin tune oscillation.* The synchrotron motion induces a spin tune oscillation, via the horizontal dispersion function, following [12]

$$\delta\nu_{\rm s} = \frac{1+G\gamma}{\pi}\Delta D'\frac{\Delta p}{p}, \tag{9}$$

with $\Delta D'$ the difference in the dispersion function derivative at the two snakes. This effect may induce multiple crossing of the resonance if the ac dipole frequency sweep is too slow, which causes polarization loss (the effect is addressed in detail in Sec. IV D).

A dedicated optical correction is used in RHIC to minimize $\Delta D'$ during the ac dipole frequency sweep [6,13]. This is further discussed in Sec. III.

## III. WORKING HYPOTHESES

RHIC spin flipper experiments were performed at injection energy, $G\gamma = 45.5$, or 23.8 GeV, and at store energy, $G\gamma = 487.3$, or 255 GeV. The details of the experimental conditions and results can be found in Ref. [4]. RHIC optics, rf, and proton bunch parameters in the present simulations are set accordingly for the sake of a realistic modeling of the experiment, in virtue of two goals of the present simulations, namely, (i) to serve as a guidance for future spin flipper experiments and (ii) ensuring effectiveness of spin simulation tools according to the needs of polarization studies in EIC ring design studies. The simulation hypotheses are detailed hereafter, various aspects are further addressed in Sec. II and in Appendix A, RHIC parameter settings are given in Table I.

TABLE I. RHIC optics, rf, and bunch settings. These are the settings in the simulations, closely reproducing APEX lattice, RF, and bunch properties. The indices 9 and 197 of the double-rf system voltages and synchronous phase and frequency refer to the 9.4 MHz and 197 MHz, respectively.

| | | Injection | Store |
|---|---|---|---|
| Energy | (GeV) | 23.81 | 255 |
| $G\gamma$ | | 45.5 | 487.3 |
| $B\rho$ | (T m) | 79.37 | 850.6 |
| Momentum compaction | ($10^{-3}$) | 1.95 | 1.92 |
| Tunes $\nu_x$; $\nu_y$ | | 28.695; 29.687 | 28.689; 29.684 |
| Chromaticities $\xi_x$; $\xi_y$ | | 5; 5 | |
| $\beta_x^*$; $\beta_y^*$, at IP6 | (m) | 10; 10 | 1.4; 1.4 |
| *Double-rf system:* | | | |
| $f_{\rm rf}$ | (MHz) | 9.4 and 197 | |
| $f_{\rm rf}/f_{\rm rev}$ | | 120 and 2520 | |
| Voltages $V_9$; $V_{197}$ | (kV) | 22; 10 | 30; 15 |
| Synchronous phase $\phi_9$ | (rad) | $\pi$ | |
| Synchronous frequency $f_s = \frac{\Omega_9}{2\pi}$ | (Hz) | 6.5 | 5.1 |
| *Bunch emittances, length, momentum spread:* | | | |
| $\beta\gamma\epsilon_{x,y}$, rms | ($\pi$μm) | 2.5 | |
| Length, full | (ns) | ±15 | |
| $\delta p/p$, full | ($10^{-3}$) | ±1.5 | ±0.25 |

### A. Orbit

The spin flipper is designed to ensure the absence of vertical orbit perturbation, as this would have a deleterious effect on beam polarization. This property is based on a locally closed bump (Figs. 2 and 3) [2].

In normal operation, vertical separation bumps maintain blue and yellow orbits up to 10 mm distant in all IRs at injection and in noncolliding IRs during physics store (Appendix A 1). These bumps have no effect on the spin flip dynamics (the particular case of IR10, where the separation bump covers the spin flipper region, is further addressed below).

Snakes are simulated here as a pure spin rotation with no orbital effect, hence an additional difference with APEX conditions (snake bumps are located at $s = 1153$ m and $s = 3070$ m, details in Appendix A 1). Detailed studies using 3D OPERA field maps of RHIC snakes have shown that the nonzero orbit along the snake sections has a marginal effect on spin motion [5].

Finally, it was checked that the residual orbit resulting from the stepwise tracking method [14] has negligible amplitude; introducing a random vertical orbit on the other hand has no effect on the spin flip efficiency. Details are given in Appendix B.

### B. Optical functions

Are detailed in Appendix A 1, at 23.8 and 255 GeV. The difference $\Delta D'$ in the horizontal periodic dispersion

derivatives at the two snakes, which causes spin tune spread [Eq. (9)], is controlled by modulating the dispersion function using RHIC lattice transition gamma ($\gamma_{\rm tr}$) quadrupoles [6]—this affects only weakly the rest of the optics. Experimentally, the measurement accuracy is the limit, with a minimum $\delta\Delta D' \approx 0.1$ mrad; simulationwise, however, $\Delta D'$ can be brought much closer to zero.

### C. rf Systems

Include a 9 MHz cavity, the main one for injection and acceleration, set at 22 kV at injection and 30 kV at 255 GeV. They also include a 197 MHz Landau cavity for beam stability, its voltage is set around 10 kV at injection, and 15 kV at 255 GeV. The voltage experienced by the bunch is [15] (notations and parameter values as in Table I; $\phi_{197}$ is defined from $\phi_9$ after [[15], Eq. (5)])

$$V(\phi) = V_9 \sin(\phi + \phi_9) + V_{197} \sin\left(\frac{2520}{120}(\phi + \phi_{197})\right).$$

Longitudinal phase space portrait establishes the correlation between bunch length (measured by wall-current monitors) and momentum spread as needed here in evaluating multiple crossing parameters, see Appendix A 1.

### D. Polarized 6D bunch

The initial coordinates of the $10^3$ particles tracked are sorted at random in Gaussian initial distributions, with parameters given in Table I. The simulations in this paper are restricted to a single random seed, the same for all, for simplicity. To validate this approach, some of the resonance crossing simulations have been repeated with different seeds: it has been observed that resulting spin flip efficiencies differ by no more than 0.1%. This may not be fully negligible, considering that it is comparable to the requirements for the spin flip efficiency (presumably, of the order of 99.9%) and may justify further statistical studies. Regarding the present benchmarking goals, however, such accuracy on the simulation results is considered appropriate for (i) the understanding of run 17 APEX results, (ii) deriving optimal spin flipper parameters for future experiments at RHIC and (iii) code benchmarking.

The initial spin of the particles is taken vertical in all simulations, however, the bunch polarization at the end of the ramp may be affected by the proximity of the resonance, this effect is discussed in Sec. V C.

### E. Spin flipper

The dc rotator and ac dipole settings are detailed in Table II. The optimal value for the dc bump angle is $\psi_0 = 109°$ [it maximizes the resonance strength, Eq. (5)]. However, (i) RHIC geometrical acceptance (horizontal orbit excursion and beam size) imposes a maximum $\psi_0 = 29.9°$ at 23.8 GeV, (ii) the magnet power supply sets a 48.8° limit at 255 GeV. The ac dipole is operated at its maximum field integral in both cases, $B_{\rm osc}L = 0.01$ T m.

TABLE II. Spin flipper settings in the APEX and in the simulations. $\delta$ is the distance to the resonance at the start ($t = 0$) and end of the frequency sweep, $S_y$ is the projection of the on-momentum spin cone on the vertical axis (which coincides with the spin precession axis).

| | | Injection | Store |
|---|---|---|---|
| Energy | (GeV) | 23.8 | 255 |
| $(1 + G\gamma)/B\rho$ | $(\mathrm{T\,m})^{-1}$ | 0.5859 | 0.5740 |
| $B_{\rm dc}L$ ($L = 1.83$ m) | (T m) | 0.8905 | 1.4842 |
| $\psi_0$ [Eq. (1)] | (°) | 29.893 | 48.813 |
| $B_{\rm osc}l$, ACD12-4 ($l = 1$ m) | (T m) | 0.01 | |
| $B_{\rm osc}l$, ACD-1, −5 ($l = 1$ m) | (T m) | 0.05 | |
| $\phi_{\rm osc}$ [Eq. (3)] | (°) | 0.3357 | 0.3289 |
| *ACD sweep parameters, APEX case* ($\Delta\nu_{\rm osc}$ *was fixed*): | | | |
| $\Delta\nu_{\rm osc}$ range | | 0.005 | |
| $\lvert\delta\rvert = \lvert\nu_s - \nu_{\rm osc}\rvert_{t=0} = \Delta\nu_{\rm osc}/2$ | ($\epsilon$) | 10.4 | 4.4 |
| $\bar{S}_{y,t=0} = \delta/(\epsilon^2 + \delta^2)^{1/2}$ | | 0.995 | 0.975 |
| $\Delta D'$ | (mrad) | 3.45 | 0.1 |
| Sweep duration $\tau_X$, optimal | (s) | 1[a] | 0.20[b] |
| Residual strength $\epsilon$ [Eq. (5)] | ($10^{-4}$) | 2.396 | 5.679 |
| $\alpha = \Delta\nu_{\rm osc}/2\pi\tau_X f_{\rm rev}$ | ($10^{-8}$) | 1 | 3.4 |
| $T$ [Eq. (8)] | (s) | 0.06 | 0.008 |
| Up and down ramps | (turn) | 120 000 | |

[a]From fit of *measured* $P_f/P_i(\tau_X)$ with Eq. (13) (Fig. 9).
[b]From fit of *simulated* $P_f/P_i(\tau_X)$ with Eq. (13) (Fig. 10).

The spin flipper is located 50 m upstream of RHIC blue IP10, in the rising region of the IP vertical orbit separation bump. The latter causes the stable spin precession direction in the flipper region (when it is off) to be tilted with respect to the vertical, by about 1.8° and 2.6° at 23.8 and 255 GeV, respectively (Appendix A 1). Dedicated simulations have shown that this has no sensible effect on the spin flip dynamics [5], it is ignored in the simulations anyway as these IP bumps are not excited, as mentioned earlier.

### F. The resonance strength

In the computer model has been assessed by an interpolation using the Froissart-Stora formula, on a series of spin flips with various crossing speeds, Fig. 4, yielding $\epsilon = 2.34 \times 10^{-4}$ at 23.8 GeV and $\epsilon = 5.60 \times 10^{-4}$ at 255 GeV. The agreement with the strength from Eq. (5), Table II, is good. Note that this is necessary for the simulations to provide guidance for future experiments.

### G. Dispersion at RHIC snakes

The difference of the dispersion function derivatives ($\Delta D'$) at the two snakes is reduced using the $\gamma_{\rm tr}$ quadrupoles [6]. $\Delta D'$ has been decreased to 3.45 mrad (±0.16 mrad accuracy) at 23.8 GeV (from ≈70 mrad) prior to any adjustment in the simulation model and to 0.1 mrad (±0.1 mrad accuracy) at 255 GeV (from 45 mrad) [13].

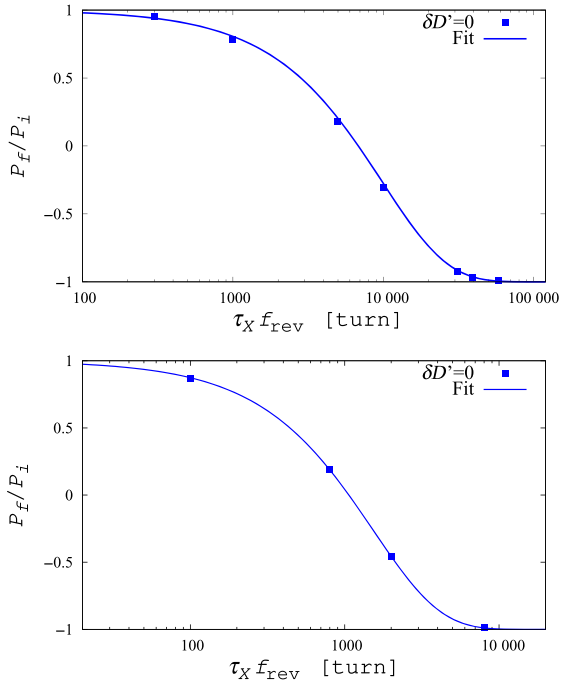


FIG. 4. Spin-flip efficiency at 23.8 (top) and 255 GeV (bottom), as a function of the number of turns of the frequency sweep over $\Delta\nu_{\rm osc} = 0.005$, from simulations (markers). A fit with the Froissart-Stora formula [Eq. (7)] (solid line) yields the resonance strength, in agreement with Eq. (5) (Table II) at $10^{-3}$ accuracy.

The effect on RHIC optics is marginal (Appendix A 1). The effect on spin flip efficiency will be discussed in the next section. Maximizing the spin flip ($P_f/P_i \to -1$) imposes $\Delta D' \to 0$ as the working value [Eq. (9)]. As low as $\Delta D' \approx 10^{-3}$ mrad is achieved by an appropriate change of the $\gamma_{\rm tr}$ quadrupoles settings, a lower limit of simulation accuracy.

## IV. PRELIMINARY SIMULATIONS

This section first comments on various basic results of spin motion and resonance crossing simulations, which can be considered a preliminary validation of the working hypotheses and tracking method, and will be referred to in the next sections.

### A. Spin tracking samples

Typical of the simulations performed in the next section are shown in Fig. 5. The observation point is IP6. Bunch polarization at any turn is obtained as a sum of the individual particle vertical spin components.

Unless otherwise indicated, the measured spin tune during the APEX was 0.4962 at 255 GeV and 0.5023 at 23.8 GeV. It is adjusted by changing the angle $\phi_2 - \phi_1$ between the snake precession axes, by virtue of [16]

$$\nu_{\rm s} = \frac{1}{\pi}\sum_{k=1,2}(-)^k\phi_k \tag{10}$$

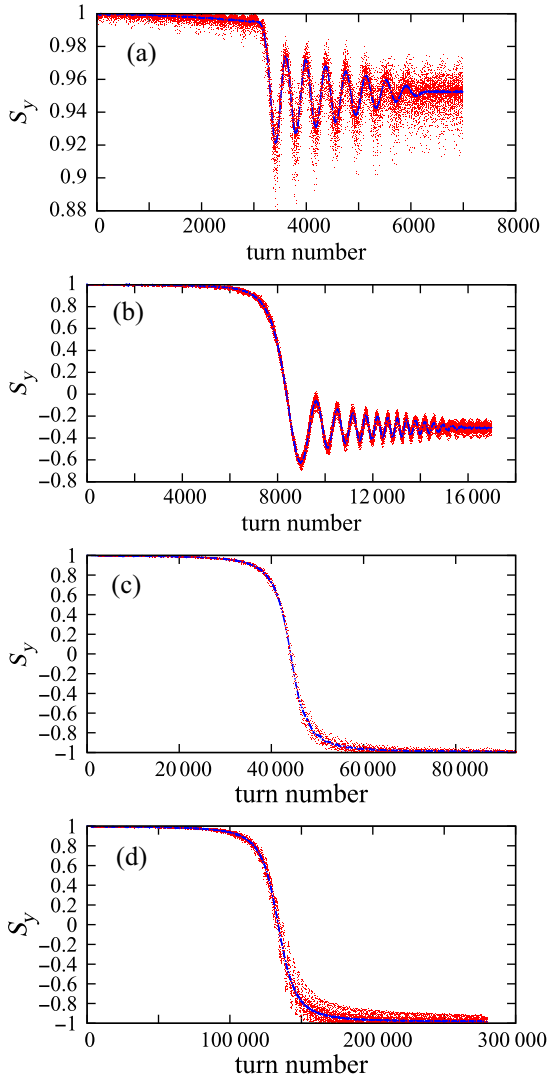


FIG. 5. Sample resonance crossings at 23.8 GeV with $\Delta D' \approx 0$. From top (a) to bottom (d), crossing duration $\tau_X = 7000,\ 17\,000,\ 86\,000,\ 273\,000$ turns. Red: spin motion of a few single particles, blue: bunch polarization, averaged over $10^3$ particles.

(with nominal $\phi_1 = -\phi_2 = 45°$ for $\nu_{\rm s} = 1/2$, in RHIC). In the simulations, $\nu_{\rm s}$ is monitored using a discrete Fourier transform on the horizontal plane spin components, with flipper turned off [Fig. 6(a)].

### B. Sweep rate

Figure 5 also illustrates the existence of an optimal sweep rate between the Froissart-Stora regime and a regime of multiple resonance crossing. The ac dipole frequency sweep duration $\tau_{\rm X}$ has been varied between 0.5 and 3.0 s in the APEX, in searching an optimum value presumed to be below a second [7]. An optimal value (i.e., at best flip efficiency) was measured to be $\tau_{\rm x} \lesssim 1$ s at 23.8 GeV, $\tau_{\rm x} < 1$ s at 255 GeV [4], see Sec. V.

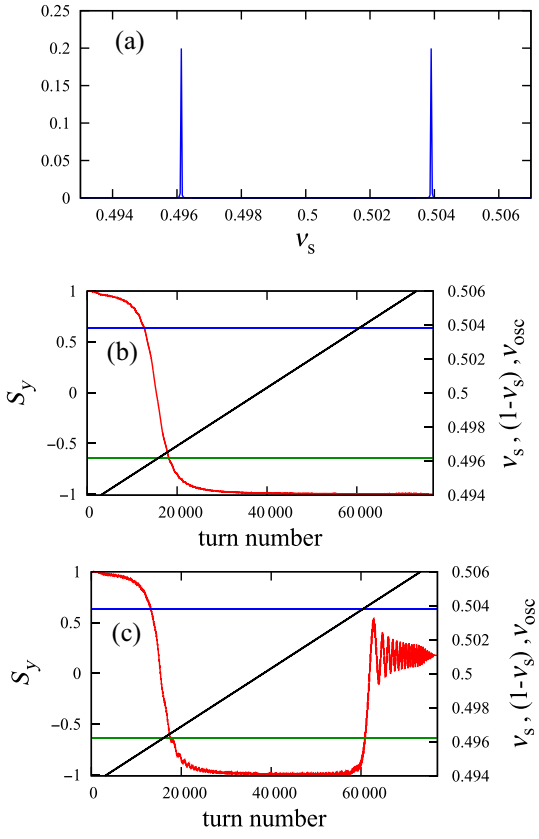


FIG. 6. (a) Sample Fourier spectrum of spin motion at 255 GeV. (b) Case of optimal spin flipper setting, ramping the ac dipole frequency over $\nu_{osc}: 0.494 \rightarrow 0.506$ (right vertical axis, oblique curve), the spin (left vertical axis) flips at $\nu_{osc} = \nu_s = 0.4962$, the mirror resonance at $\nu_s = 0.5038$ is not excited. (c) A case of mis-setting of the relative ACD1-3-ACD3-5 bumps phase [Eq. (4)], namely $\psi_0 = 30$ (the nominal value at 255 GeV is $\psi_0 = 48.7°$, Table II), the image resonance is excited, causing partial flip.

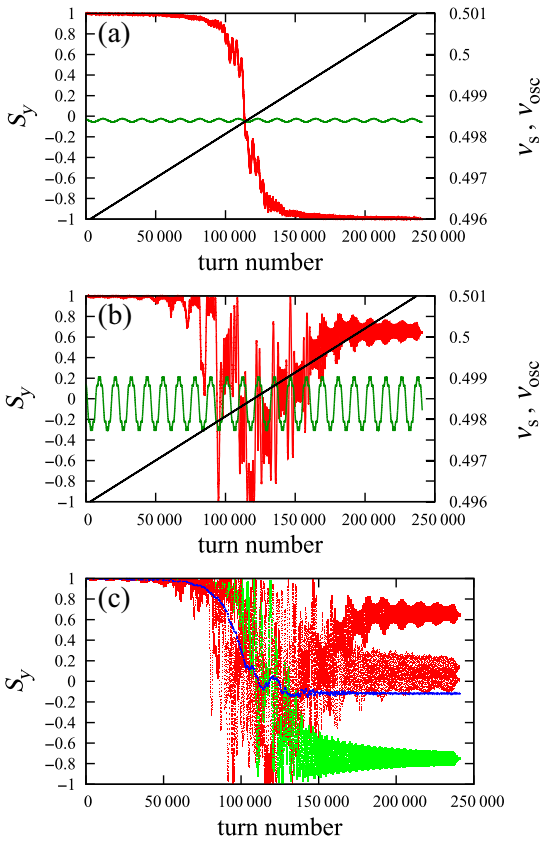


FIG. 7. (a) Single crossing, avoiding long neighboring of $\nu_s$ and $\nu_{osc}$, requires $d\nu_{osc}/dt \gg \max(d\nu_s/dt)$. (b) A large $\Delta D' = 44$ mrad causes a large spin tune oscillation $\delta\nu_s$ [Eq. (9)] resulting in multiple crossing. The number of crossing reaches a maximum if $\Delta\nu_{osc} < 2\delta\nu_s$. (c) Sample spin motion and (blue) average polarization for a $10^3$ particle bunch, case $\Delta D' = 44$ mrad. Note the spin oscillations in the early times in (b) and (c), an indication that the $\nu_{osc}$ sweep should start and end further distant from $\nu_s$.

### C. Mirror resonance

Single particle spin tracking is carried out here to illustrate the spin dynamics. Figure 6(b) is obtained with optimal spin flipper setting, showing spin flip when the driving tune crosses the spin tune (location of the artificial resonance), whereas there is no effect upon crossing the mirror resonance at $1 - \nu_s$. Possible ways to excite the mirror resonance include misclosed ACD vertical bump; a difference in the frequency range of the two ACD bumps; mis-setting of the ACD1-3–ACD3-5 relative phase [Eq. (4)]. Partial spin flip in the latter case is illustrated in Fig. 6(c).

These simulations confirm the importance of suppressing the mirror resonance.

### D. Multiple resonance crossings

The sizable spin tune oscillations [Eq. (9)] are expected to cause multiple crossing during the frequency sweep $\nu_{osc}(t)$. Single particle and multiple particles simulations confirm this effect, as shown in Fig. 7. A single crossing occurs if the spin tune oscillation is much slower than the driving tune sweep speed, namely, $d\delta\nu_s/dt \ll d\nu_{osc}/dt$. Taking $\delta p/p = \hat{\delta}\sin(\Omega_s t)$ and differentiating Eq. (9) yields the maximum slope of the spin tune oscillation, namely, $\frac{1+G\gamma}{\pi}\Delta D'\Omega_s\hat{\delta}$. Thus, given $d\nu_{osc}/dt = \alpha\omega_{rev}$ [Eq. (6)], multiple crossing and $\nu_{osc}$ stationing along the varying $\nu_s$ [Fig. 7(a)], are avoided if $(1+G\gamma)\Delta D'\Omega_s\hat{\delta} \ll \pi\alpha\omega_{rev}$, i.e.,

$$\Delta D' \ll \frac{\pi\alpha}{(1+G\gamma)\hat{\delta}}\frac{f_{rev}}{f_s} \approx \begin{cases} 5 \text{ mrad at } 23.8 \text{ GeV} \\ 10 \text{ mrad at } 255 \text{ GeV} \end{cases} \quad (11)$$

(numerical values from data in Tables I and II). Accounting for the width of the resonance [this is apparent in Fig. 7(b)], the maximum number of crossings is reached when the synchrotron tune oscillation exceeds a fraction of $\Delta\nu_{osc}$, i.e.,

$$\Delta D' > \text{a fraction of}\,\frac{\pi\Delta\nu_{osc}}{2(1+G\gamma)\hat{\delta}} \approx \begin{cases} 100 \text{ mrad at } 23.8 \text{ GeV} \\ 50 \text{ mrad at } 255 \text{ GeV} \end{cases}. \quad (12)$$

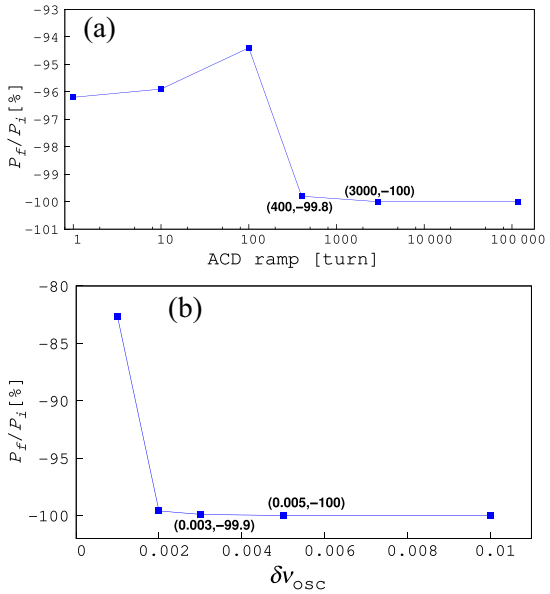


FIG. 8. Dependence of spin flip efficiency, at 255 GeV, on (a) ACD ramp duration and (b) $\Delta\nu_{\rm osc}$ (detailed values between parentheses).

### E. ac dipole up and down ramps

Were 1.5 s, 117 000 turns, in the APEX. In the simulations, the ramp is performed in 3000 turns, this is still slow enough and ensures the motion of spins toward the resonance without significant difference in asymptotic bunch polarization after the crossing. This is illustrated in Fig. 8(a) at 255 GeV, with $\Delta D' \approx 0$, optimal sweep time $\tau_X = 0.2$ s, $\Delta\nu_{\rm osc} = 0.005$. The spin flip efficiency neighbors 100% for a 1000 turn ramp and beyond, in the run 17 APEX conditions. Spin motion details can be found in Appendix C.

### F. The ac dipole frequency range

During the APEX was $\Delta\nu_{\rm osc} = 0.005$, i.e., start and end of the sweep distant $\delta = 10\epsilon$ from the resonance, at 23.8 GeV (Table II), average polarization amounts to $S_y = 0.995$. The distance is shorter at 255 GeV, $\delta = 4.4\epsilon$, or $S_y = 0.975$. At the start of the ramp, $\hat{B}_{\rm osc}(t)$ and thus the resonance strength are zero [$\phi_{\rm osc} = 0$ in Eq. (5)] and $S_y = 1$ [the equilibrium spin cone angle $\mathrm{acos}(S_y) = 0$]. During the ramp up, $\hat{B}_{\rm osc}(t)$ is slowly brought to its peak value so that spins move coherently and $S_{y,t=0} = \delta/(\epsilon^2 + \delta^2)^{1/2}$ (and similarly the other way, on the ramp down). As a consequence, increasing $\Delta\nu_{\rm osc}$ (and thus $|\delta| = |\nu_s - \nu_{\rm osc}|_{t=0}$) is not expected to have substantial effect on spin flip efficiency. This is illustrated in Fig. 8(b), the spin flip efficiency neighbors 100% for $\Delta\nu_{\rm osc}$ around 0.003 and beyond, in the run 17 APEX conditions. Spin motion details can be found in Appendix C.

## V. SIMULATION OF RUN 17 EXPERIMENTS

RHIC and spin flipper parameters during the APEX are summarized in Tables I and II. The simulations focus on reproducing quantities that can be extracted from RHIC run 17 APEX measurements, the details and results of which can be found in [4]. Extrapolations from simulations that closely reproduce the measurements are used to derive the expected optimal spin flipper settings at 23.8 and 255 GeV.

### A. Crossing rate

APEX measurements and simulation outcomes are compared in Figs. 9 (23.8 GeV) and 10 (255 GeV). Note that numerical simulations in both cases are done with small $\Delta D'$ values which, by virtue of Eq. (11), exclude multiple crossing, therefore, if any loss of polarization, the cause is not multiple crossing.

In the 23.8 GeV case where several measurements of $P_f/P_i(\tau_X)$ are available, the agreement is within a satisfactory 10%. The deviation from the Froissart-Stora formula is greater with longer sweep time, $P_f/P_i$ appears to increase linearly for $\tau_X$ values beyond the location $\tau_{X,\rm min}$ of the optimal spin flip efficiency (additional simulations with various values of $\Delta D'$, not shown here, confirm this feature). This suggests an interpolation using a linear combination of (i) Eq. (7) for the fast sweep region (smaller sweep duration $\tau_X$ and faster crossing speed) and (ii) a linear increase for the slow sweep region (larger $\tau_X$), namely,

$$\frac{P_f}{P_i}(\tau_X) = 2\,\exp\left(-\frac{\tau_X}{2T}\right) - 1 + \frac{\tau_X}{a}. \tag{13}$$

Tracking simulations allow determining the slope $1/a$. By differentiation with respect to $\tau_X$, and noting

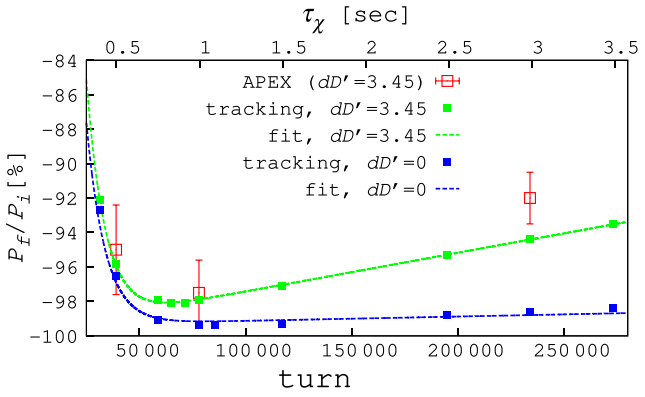


FIG. 9. Dependence of spin flip efficiency on sweep time duration, for different $\Delta D'$ values, including measured (red, empty squares) and simulated (solid markers) data, at 23.8 GeV. The linear shape of $P_f/P_i(\tau_X)$ at large $\tau_X$ values suggests an interpolation (dashed curves) using Eq. (13). Note that the rightmost blue marker (respectively, the fifth one from the right) corresponds to the simulation of Fig. 5(d) (respectively Fig. 5(d)).

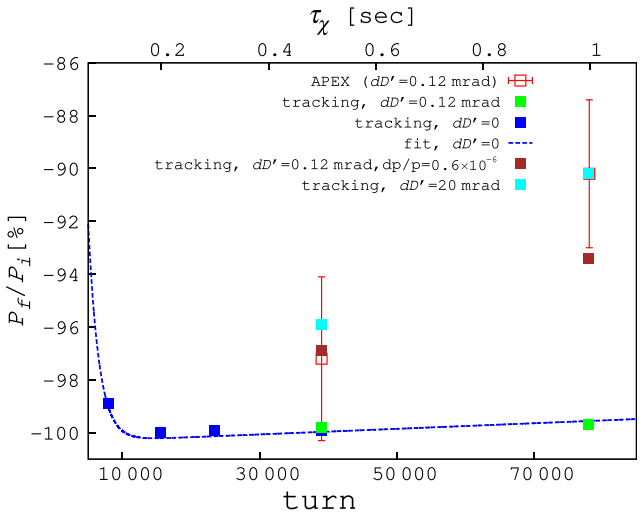


FIG. 10. Dependence of spin flip efficiency on sweep time duration and on $\Delta D'$, including measured (red, empty squares, $\Delta D' = 0.12$ mrad at $\tau_X = 38\,000$ and $78\,000$ turns) and simulated data (solid squares, $\Delta D' = 0$), at 255 GeV. Interpolation of the latter (dashed blue curve) using Eq. (13) yields the best efficiency, $P_f/P_i = -99.9$, for $\tau_X = 16\,000$ turns (a 0.20 s sweep). At turn = 38 000 and 78 000, the two cases $\Delta D' = 0$ and $\Delta D' = 0.12$ mrad overlap, straddling the interpolation curve, this is an indication of a less stringent constraint on $\Delta D' \to 0$ at higher energy [as expected from Eq. (11)]. As the tracking results for a 38 000 and a 78 000 turn sweep are very similar, whether $\Delta D' = 0$ or 0.12 mrad, no further simulations were performed for smaller $\tau_X$ in the latter case.

$\tau_{\mathrm{X,min}} = \tau_X[\mathrm{Max}|P_f/P_i|]$, this yields the optimum sweep time duration

$$\tau_{\mathrm{X,min}} \approx 2T\ \ln(a/T). \tag{14}$$

This empirical approach to $\tau_{\mathrm{X,min}}$ proves efficient and allows saving on time-consuming computing trials, when performing tracking simulations aimed at accurate identification of $\tau_{\mathrm{X,min}}$, a critical parameter in devising the ac dipole settings.

This $|P_f/P_i|$ decrease for $\tau_x > \tau_{\mathrm{X,min}}$ is attributed to the slow synchrotron motion that causes particles from the bunch to slowly span their momentum excursion range $\pm\hat{\delta}$ (up to $\pm 2 \times 10^{-3}$ for great longitudinal invariant, see Appendix A 3). This causes a slow spin tune oscillation [Eq. (9)], with the latter causing polarization loss during resonance crossing [12]. The synchrotron period is $\approx$2 s, longer than the optimal sweep duration $\approx$1 s, increasing with greater longitudinal invariant. As a consequence, the timescale to $\pm\hat{\delta}$ is several $\tau_{\mathrm{X,min}}$, during which polarization loss builds up. Quantifying this effect requires more insight, it should allow clarifying such aspects as the dependence of $\tau_{\mathrm{X,min}}$ or $\mathrm{Max}|P_f/P_i|$ on $\Delta D'$, a work in progress.

The optimum sweep time duration increases with decreasing $\Delta D'$, in particular $\tau_X \to \infty$ for $\Delta D' \to 0$ as in that case $P_f/P_i$ is a monotonically decreasing function of $\tau_X$ following Froissart-Stora law (Fig. 9). However in that case, the experimental value for the sweep duration would be determined from the spin flipper capabilities on the one hand and on a maximum desirable value of $|P_f/P_i|$ (of the order of 99.9% for instance, for ten flips in a run, as aforementioned). When $\Delta D' = 0$ is increased, $P_f/P_i$ features a minimum, the efficiency worsens at all $\tau_X$ and $\tau_{\mathrm{X,min}}$ decreases.

Table III displays the numerical outcomes for various $\Delta D'$ values, including an optimal $\tau_X \approx 0.9$ s for $\Delta D' \approx 0$. In this case, $\min(P_f/P_i)$ is only weakly dependent on $\tau_X$ (Fig. 9); it can be noted, however, that even though $\Delta D' \approx 0$ [i.e., absence of multiple crossing, see Eq. (12)], the flip efficiency slowly deteriorates with increasing $\tau_X$ beyond $\tau_{X,\mathrm{min}}$. This is no longer the case if the rf is set off [as $\delta\nu_s = 0$ following Eq. (9)—note that rf off is only possible in the simulations]: in that case, $\min(P_f/P_i)$ satisfies the Froissart-Stora formula with $P_f/P_i = -1$ as an asymptote.

Following these simulations, crossings with wider driving tune sweep $\nu_{\mathrm{osc}} = 0.01$ were performed for both 23.8 and 255 GeV, however, this shows only a marginal effect on spin flip efficiency.

Attempts were made to explain the discrepancy between measurements and simulations at $\tau_X = 1$ s (78 000 turns) at 255 GeV, as shown in Fig. 10, namely, a measured 90% efficiency, compared to close to 100% from the simulations. Attempts included introducing a random vertical orbit (approximately 1 mm in the arcs) or introducing a misclosure of the vertical ACD bump; however, neither yielded such a large discrepancy. On the other hand, using a higher momentum spread $\delta p/p$ in the bunch and higher rf voltage does give a better agreement with the measured data, however, such beam conditions are likely not the explanation, as they are much larger than recorded values during the experiment.

TABLE III. Dependence of the optimal sweep duration (column 2) on $\Delta D'$ (column 1). Corresponding $P_f/P_i$ values are added in various simulation cases (column 4), giving a guidance regarding expected efficiency of the spin flipper, and in the APEX case for comparison (column 3).

| | | Optimum $P_f/P_i$ | |
|---|---|---|---|
| | | APEX | simulation |
| $\Delta D'$ (mrad) | $\tau_{X,\mathrm{min}}$ (s) | (%) | |
| 23.8 GeV | | | |
| 3.45 | 0.73 | −97.8 | |
| 3.45 | 0.78 | | −98.2 |
| 3 | 0.77 | | −98.3 |
| 0 | 0.90 | | −99.4 |
| 255 GeV | | | |
| 0.1 | <1 | $\lesssim -97.2$ | |
| 0 | 0.90 | | −100 |

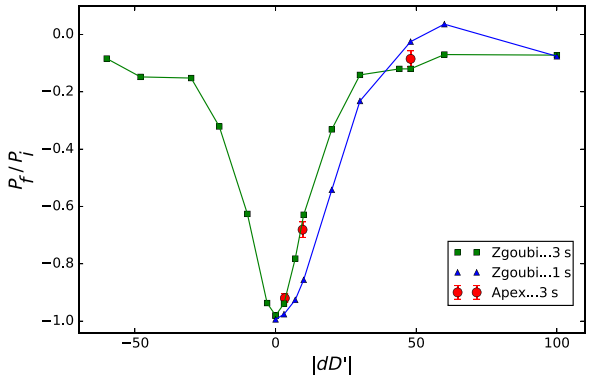


FIG. 11. Dependence of $P_f/P_i$ on $\Delta D'$ at 23.8 GeV ($G\gamma = 45.5$), with $\Delta\nu_{\rm osc} = 0.005$. The measured data were for $\tau_X = 3$ s and simulations were for $\tau_X = 1$ and 3 s. The latter yield best flip efficiency $P_f/P_i = -99.4$. Increasing $\Delta\nu_{\rm osc}$ changes the efficiency by less than 0.1.

### B. Spin tune spread

#### 1. $\Delta D'$ dependence

Spin tune spread in a bunch decreases in proportion to $\Delta D'$, as seen in Eq. (9). Spin flip efficiency was measured at 23.8 GeV for various spin tune spread values due to different $\Delta D'$ values. The spin flip efficiency from APEX data and numerical simulations is plotted in Fig. 11. The agreement between experimental data and simulations is very good. Comparison between 1 and 3 s sweep times shows that faster sweep time can improve the spin flip efficiency. $\Delta D'$ appears as an efficient parameter for improving the spin flip efficiency, by bringing it closest to zero [13]. These results are consistent with the asymptotic behavior discussed earlier which indicates [Eq. (12)] a flat $P_f/P_i(\Delta D')$ for $|\Delta D'|$ beyond a few tens of mrad at 23.8 GeV.

### C. Partial resonance sweep

Incomplete flip occurs if the $\Delta\nu_{\rm osc}$ swing only partially covers the ac dipole induced resonance. Some of the APEX measurements happen to fall into this configuration. They are considered, too, an opportunity for additional simulations and further benchmarking.

#### 1. Spin tune

The APEX included measurements with the Siberian snake currents set at 321 and 95 A which theoretically corresponds to $\nu_s = 0.4968$ [5]. The nominal currents are 323 and 100 A (this theoretically yields $\nu_s = 0.4982$). The difference in the snake settings should result in a spin tune shift of $\delta\nu_s = -0.0014$.

The spin tune at 255 GeV was measured for the nominal snake settings (323 and 100 A) to be $\nu_s = 0.496125 \pm 0.000257$ [17]. The spin tune for snake currents of 321 and 95 A was not measured, but it should be around $\nu_s = 0.4947$, if we consider how the spin tune depends on the snake settings.

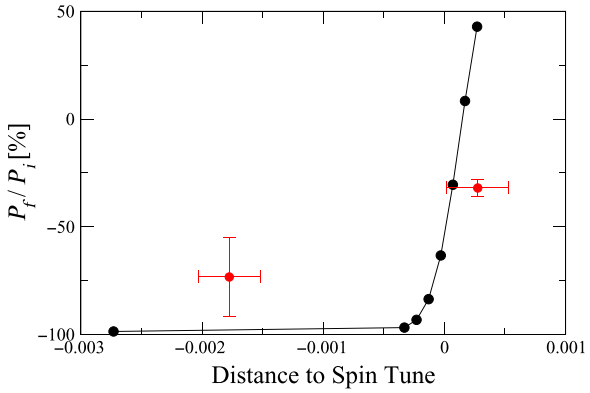


FIG. 12. Partial resonance sweep. The spin-flip efficiency depends on how far the spin tune is outside of the oscillator range. "Distance to spin tune" is defined as the lower limit of the oscillator range minus the spin tune. The oscillator range is 0.005, $\Delta D' = 3$ mrad, $\tau_X = 3$ s at 255 GeV. Red: measured data; Black: simulations.

#### 2. Spin flip

Two spin-flip measurements were performed successively at 255 GeV, with $\Delta D' = 3$ mrad, sweep time $\tau_X = 3$ s, and $\Delta\nu_{\rm osc} = 0.005$. During the first spin flip, the ac dipole frequency range was set to 0.495–0.500, which does not cover the whole resonance (given $\nu_s = 0.4947$). A spin-flip efficiency $P_f/P_i = (-32 \pm 4)\%$ was measured.

The ac dipole frequency range was changed to 0.493–0.498 yielding a spin-flip efficiency $P_f/P_i = -78 \pm 20\%$ for the second spin flip.

#### 3. Simulations

A series of simulations with various distances between driving oscillation and spin tune have been performed regarding the first and the second spin flip, showing reasonable agreement with the measured values: due to spin tune spread, part of the beam is still affected by the sweep, and a sharp change in spin-flip efficiency should occur when the distance to spin tune increases. This is

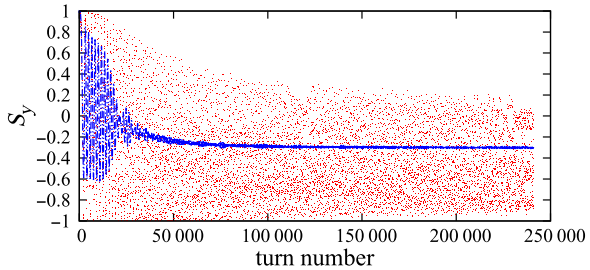


FIG. 13. Simulation of the spin flip when the whole resonance is not covered, causing an asymptotic polarization of $P_f = -0.3$, from an initial $P_i \approx 1$. Red: vertical spin component of individual particles; Blue: average vertical spin component of the $10^3$ particles.

observed in both experiment and simulations, Fig. 12. Figure 13 is an illustration of the way the polarization is affected during the partial sweep—the distance to the spin tune is 0.001 in this case.

## VI. CONCLUSIONS

Numerical simulations agree well with APEX results at both 23.8 and 255 GeV. To summarize: (i) A necessary condition for nearing 100% spin-flip efficiency is a negligible difference in the derivative of the dispersion function at the two Siberian snakes, $\Delta D' \to 0$. This is a consequence of multiple resonance crossing, an effect that dominates for slow sweep rate $\alpha$. The simulations, supported by their good accord with experimental data, allow quantifying that effect and establishing a threshold for $\Delta D'$ given a target efficiency. (ii) The Froissart-Stora formula dominates the flip efficiency in the case of fast crossing and sets a higher limit for $\alpha$. (iii) Between these two effects, there is an optimal resonance crossing speed that yields an extremum $P_f/P_i \to -1$. (iv) A wide enough $\Delta\nu_{\rm osc}$ is necessary to set the start and end of the sweep range away enough from the resonance for the Froissart-Stora formula to apply. The numerical simulations allow establishing a threshold value for $\Delta\nu_{\rm osc}$. (v) The ramps up and down, to and from $\max(\hat{B}_{\rm osc})$ can be short, of the order of a few thousand turns.

The experimental results can be explained by simulations with realistic lattice and beam parameters. With these benchmarking results, the simulation tool can provide guidance for improvement of spin-flip efficiency in future experiments at RHIC.

## ACKNOWLEDGMENTS

For these RHIC spin flipper model developments, extensive tracking simulations were performed on NERSC computers [18], a much valuable tool. Work supported by Brookhaven Science Associates, LLC under Contract No. DE-AC02-98CH10886 with the U.S. Department of Energy.

## APPENDIX A: RHIC OPTICS

### 1. Orbit

In the simulations, orbit aspects that are of no or negligible effect on the spin-flip dynamics are ignored. This includes (i) absence of orbit separation bumps at IPs: the IP and snake bumps are zeroed (by contrast with normal RHIC configuration in Fig. 14), (ii) absence of separation bump at IP10 where the spin flipper is located, in a region where, due to that bump, the stable precession direction $\vec{n}_0$ is vertically tilted by about 2° (Fig. 15), (iii) using pure spin rotation to simulate the snakes, so ignoring the local vertical orbit bump, they induce and its compensation,

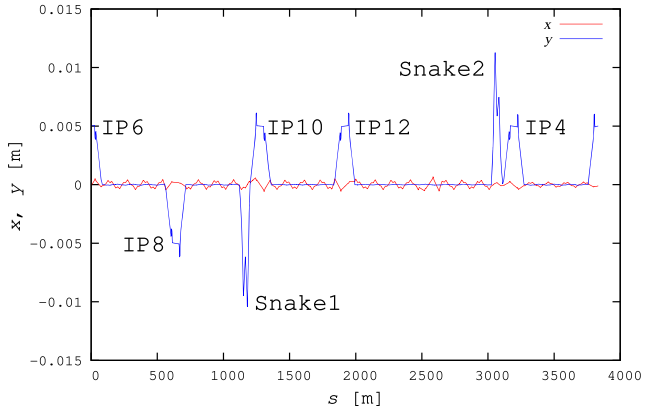


FIG. 14. Vertical design orbit at injection in the RHIC run 17 optics model, including separation bumps at IP6, 8, 10, 2, 4, and snake orbit bumps in the $s = 1153$ m and $s = 3070$ m regions. All these bumps are zeroed in the simulations.

as well as the spiraling motion across the helical dipoles [5].

### 2. Optical functions

The optical functions in the simulations are displayed in Fig. 16. A particularity of the APEX optics is in the

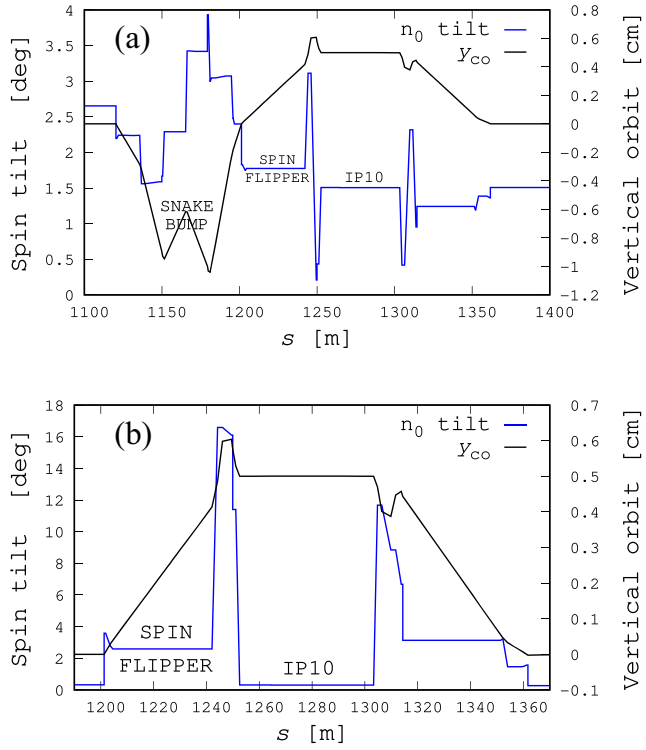


FIG. 15. The spin flipper extends over $1213 \lesssim s \lesssim 1231$ m in the raising region of the vertical orbit separation bump (the $y_{\rm co}$ curve, right vertical axis) at RHIC IP10. There the spin is vertically tilted (left vertical axis) by ≈1.8° at injection (a), ≈2.6° at store (b) [5].

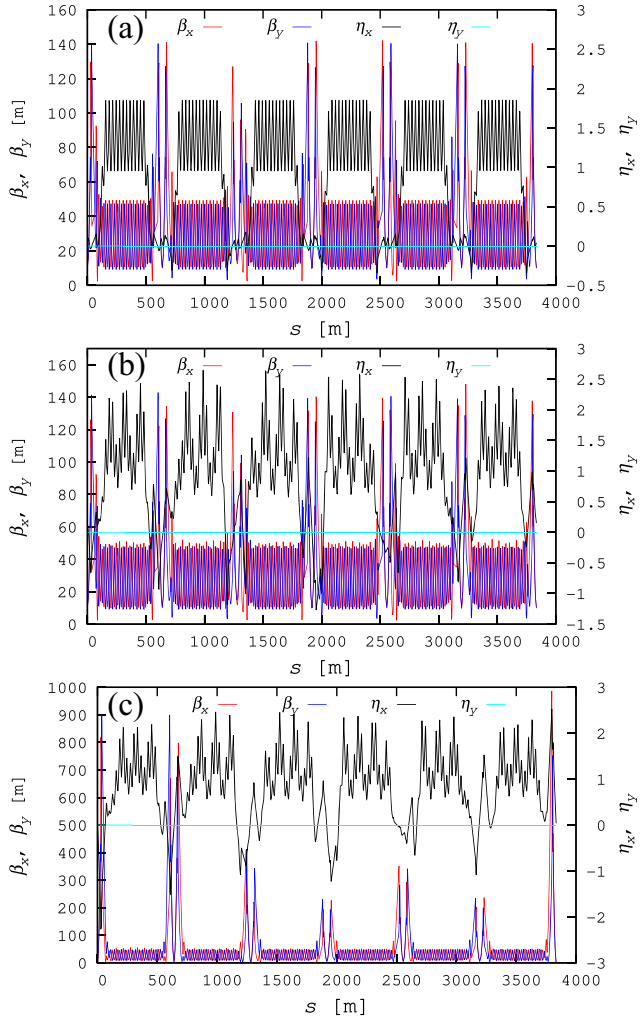


FIG. 16. RHIC blue optics. (a), (b) at injection, $\nu_x = 28.695$, $\nu_y = 29.687$, $\beta^*_{x,y} = 10$ m, $\xi_{x,y} \approx 5$; (c) at store, $\nu_x = 28.689$, $\nu_y = 29.684$, $\beta^*_{x,y} \approx 1.4$ m, $\xi_{x,y} \approx 5$. In (a), case of regular operation optics, the transition gamma quadrupoles are off, $D_x(s)$ is not modulated, $D'_x(s)$ values at snake 1 and snake 2 differ by 63 mrad. In (b) and (c), the horizontal dispersion is modulated under the effect of the transition gamma quadrupoles, set in this example to bring $|\Delta D'|$ down to, respectively, 13 and 9 mrad.

modulation of the dispersion function, by the transition gamma quadrupoles as they are used to control $D'_x$ at both RHIC snakes.

Note that RHIC detector magnets, STAR (solenoid) and PHENIX (a dipole oriented with field longitudinal) are absent from the simulations. Their effect on the stable spin precession axis $\tilde{n}_0$ is, however, negligible [19].

### 3. Longitudinal phase space

Bunch length in RHIC is measured from wall-current monitors. The sample synchrotron motion displayed in Fig. 17 establishes the correlation with full momentum

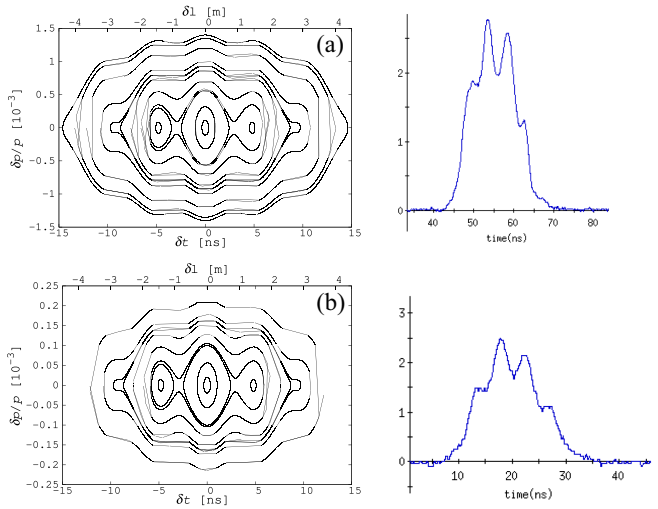


FIG. 17. Longitudinal motion. Stationary bucket (left) and wall current measurement (right), at 23.8 GeV (a) and 255 GeV (b).

excursion ($\delta p/p$) for a bunch length of about 20 ns, at both 23.8 (a) and 255 GeV (b), about $\pm 1.5 \times 10^{-3}$ and $\pm 2.5 \times 10^{-4}$, respectively. rf parameters in these simulations are essentially similar to APEX ones, as listed in Table I.

## APPENDIX B: ORBIT DEFECT CONSIDERATIONS

A residual vertical orbit oscillation is present in the simulations (a numerical effect, resulting from the ray-tracing method used to compute particle and spin motion, and from a nonperfect local bump closure at the flipper), however, with totally negligible amplitude as can be observed in Fig. 18.

Figure 19 shows that a vertical orbit defect, even large [up to ≈1 mm excursion in the arcs here, Fig. 19(a), due to a random kick in the vertical correctors], does not excite the mirror resonance. Thus, in the case of realistic random

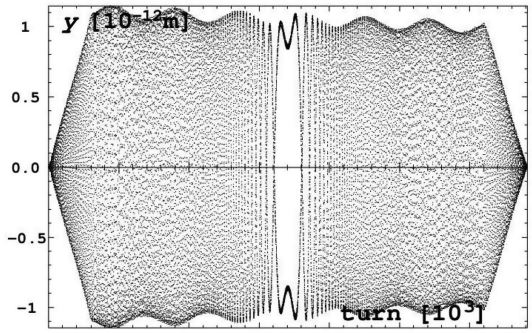


FIG. 18. Residual vertical orbit oscillation, observed at IP6 where $\beta_y = 1.4$ m, during an ac dipole frequency sweep. The oscillation amplitude is negligible: its equivalent invariant value is orders of magnitude below beam emittance.

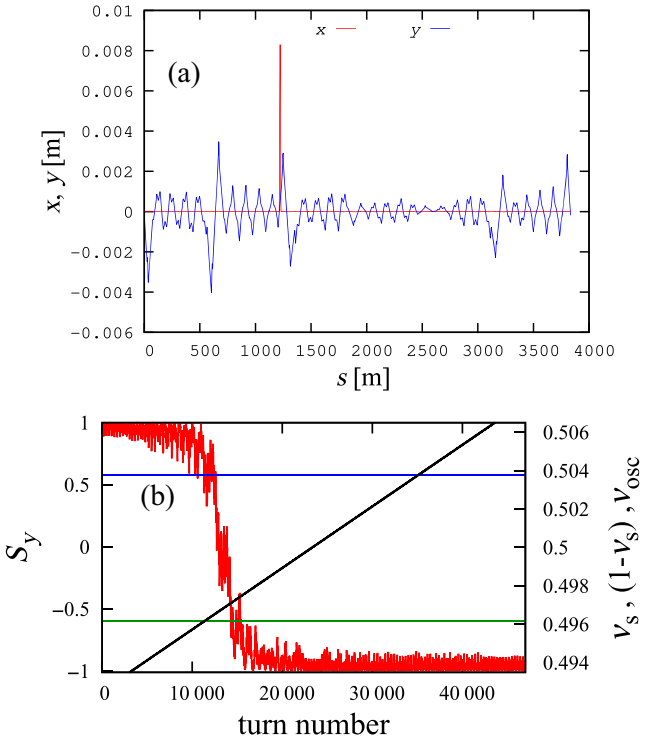


FIG. 19. (a) A vertical orbit is introduced (random kicks in RHIC correctors) causing up to ≈1 mm excursion in the arcs, blue curve (for the record, the $x$ orbit is also shown, with its local bump at the dc rotators at maximum amplitude—red curve), for 255 GeV. (b) The oblique (black) line represents $\nu_{\mathrm{osc}}$(turn). Spin flip occurs at $\nu_{\mathrm{osc}} = \nu_{\mathrm{s}} = 0.4965$ (intersection with the green line), no effect on spin at $1 - \nu_{\mathrm{s}} = 0.5035$ (red line): the vertical defect orbit does not excite the mirror resonance.

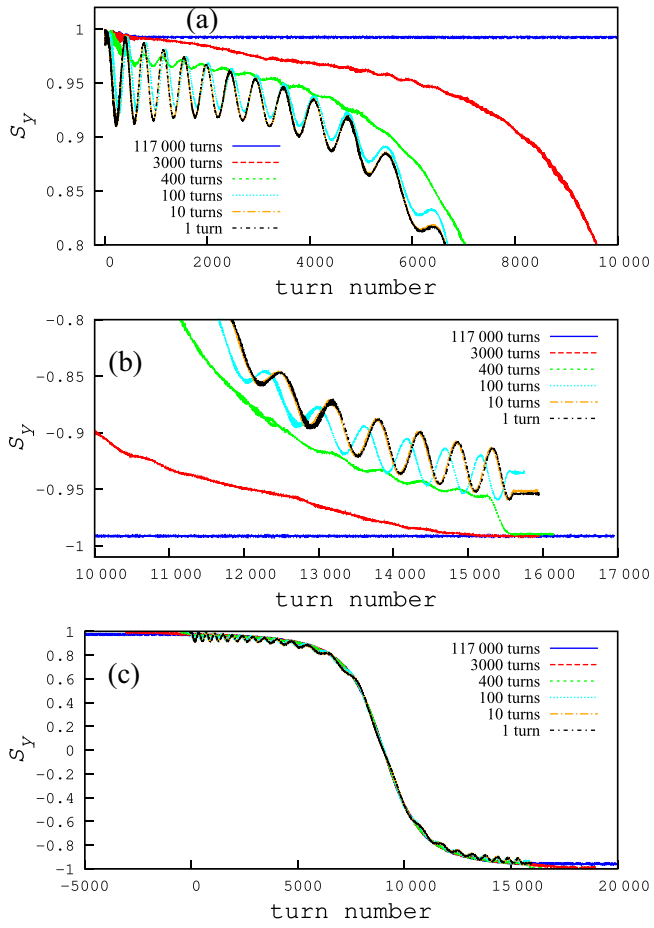


FIG. 20. (a) Region of the start of the ramp (at turn 50) and the effect of its duration. Energy is 255 GeV here. (b) Region of the end of the ramp (at turn 15 600) and the effect of its duration. (c) Complete crossing.

vertical orbit defect (of the order of a few tens of micrometers, rms), departure of $\nu_{\mathrm{s}}$ from $\frac{1}{2}|$ would not entail a double crossing.

## APPENDIX C: RAMP DURATION; DISTANCE TO THE RESONANCE

Figure 20(a) shows the effect on spin motion of the duration of the up ramp. Oscillations essentially disappear for 3000 turns and beyond. The origin on the horizontal axis is the beginning of the tracking. Figure 20(b) shows the down ramp region, with the ramp ending at turn 15 600. Oscillations essentially disappear for 3000 turns and beyond. The figure also shows that the final polarization (beyond turn 15 600) correlates with the phase of the oscillation at the end of the ramp. It can be concluded that 3000 turns as used in the simulations does not affect the spin-flip efficiency, whereas it reduces the simulation time.

Figure 20(c) shows the complete crossing. It can be observed that, for the various ramp up durations, the core of the frequency sweep remains identical.

[1] The Electron-Ion Collider. A machine that will unlock the secrets of the strongest force in nature, https://www.bnl.gov/eic/.

[2] M. Bai and T. Roser, Full spin flipping in the presence of full Siberian snake, Phys. Rev. ST Accel. Beams **11**, 091001 (2008).

[3] M. Bai *et al.*, RHIC spin flipper status and simulation studies, in *Proceedings of the 24th Particle Accelerator Conference, PAC-2011, New York* (IEEE, New York, 2011).

[4] H. Huang, J. Kewisch, C. Liu, A. Marusic, W. Meng, F. Méot, P. Oddo, V. Ptitsyn, V. Ranjbar, and T. Roser, High spin-flip efficiency at 255 GeV for polarized protons in a ring with two full Siberian snakes, Phys. Rev. Lett. **120**, 264804 (2018).

[5] F. Méot *et al.*, Re-visiting RHIC snakes—OPERA fields, $\tilde{n}_0$ dance, BNL, Technical Note No. BNL C-A/AP/590, https://technotes.bnl.gov/PDF?publicationId=42159.

[6] J. Kewisch *et al.*, Correction of the spin chromaticity in RHIC, BNL, Technical Note No. BNL C-A/AP/478, 2013, https://technotes.bnl.gov/PDF?publicationId=32232.

[7] F. Méot *et al.*, RHIC Spin flipper, fast-sweep efficiency simulations, BNL, Technical Note No. 56 BNL C-A/AP/589, 2017, https://technotes.bnl.gov/PDF?publicationId=42090.

[8] P. Adams *et al.*, Numerical simulation of spin dynamics with spin flipper in RHIC, in *Proceedings of the 9th International Particle Accelerator Conference, IPAC-2018, Vancouver, BC, Canada* (JACoW, Geneva, Switzerland, 2018), https://accelconf.web.cern.ch/ipac2018/papers/mopmf018.pdf.

[9] M. Froissart and R. Stora, Nucl. Instrum. Methods **7**, 297 (1960).

[10] V. Ptitsyn *et al.*, eRHIC design status, in *Proceedings of the 9th International Particle Accelerator Conference, IPAC-2018, Vancouver, BC, Canada* (JACoW, Geneva, Switzerland, 2018), https://accelconf.web.cern.ch/ipac2018/papers/tuygbd3.pdf.

[11] Lookup RHIC, AGS, BOOSTER spin studies papers in accelerator conference proceedings, https://www.jacow.org/Main/Proceedings.

[12] M. Bai *et al.*, Impact on spin tune from horizontal orbital angle between snakes and orbital angle between spin rotators, Brookhaven National Laboratory (BNL), Upton, NY, Technical Note No. C-A/AP/334, 2008.

[13] C. Liu *et al.*, Minimization of spin tune spread by matching dispersion prime at RHIC, BNL, Report Nos. BNL-114288-2017-IR, C-A/AP/593, 2017, https://technotes.bnl.gov/PDF?publicationId=42358.

[14] https://sourceforge.net/p/zgoubi/code/HEAD/tree/trunk/guide/Zgoubi.pdf; https://www.osti.gov/scitech/biblio/1062013-zgoubi-users-guide.

[15] A. Hofmann and S. Meyers, Beam dynamics in a double RF system, CERN, Geneva, Report No. CERN ISR-TH-RF/80-26, 1980.

[16] S. Y. Lee, *Spin Dynamics and Snakes in Synchrotrons* (World Scientific, Singapore, 1997).

[17] H. Huang *et al.*, Measurement of the spin tune using the coherent spin motion of polarized protons in a storage ring (to be published).

[18] NERSC computing, on web, http://www.nersc.gov/.

[19] F. Méot *et al.*, On the effects of detector solenoids on $\tilde{n}_0$ in RHIC and eRHIC, Brookhaven National Laboratory (BNL), Upton, NY, Technical Report No. eRHIC Note 60, 2018.